Eu 3+ Coordination in an Organic/Inorganic Hybrid Matrix with Methyl End-Capped Short Polyether Chains

ARTICLE *in* THE JOURNAL OF PHYSICAL CHEMISTRY B · APRIL 2005

Impact Factor: 3.3 · DOI: 10.1021/jp045660v · Source: PubMed

Eu^{3+} Coordination in an Organic/Inorganic Hybrid Matrix with Methyl End-Capped Short Polyether Chains

V. de Zea Bermudez,*,† D. Ostrovskii,‡ M. C. Gonçalves,† S. Lavoryk,‡ L. D. Carlos,§ and R. A. Sá Ferreira§

Departamento de Química and CQ-VR, Universidade de Trás-os-Montes e Alto Douro, 5000-911 Vila Real, Portugal, Department of Physics, Chalmers University of Technology, 41296 Göteborg, Sweden, and Departamento de Física and CICECO, Universidade de Aveiro, 3810-193 Aveiro, Portugal

Received: September 24, 2004; In Final Form: January 21, 2005

Fourier Transform mid-infrared (FT-IR), Fourier Transform Raman (FT-Raman) and photoluminescence spectroscopies and Two-Dimensional (2D) Correlation Spectroscopic Analysis were employed to examine the anionic and cationic local environments in *mono-urethanesils* doped with europium triflate ($Eu(CF_3SO_3)_3$). The hybrid host framework of these materials is composed of a siliceous backbone bonded through urethane linkages to CH_3-terminated polymer chains containing about 7 OCH_2CH_2 units. Samples with $\infty \geq n$ (composition) ≥ 5 (where $n = OCH_2CH_2/Eu^{3+}$) were studied. In terms of ionic association, the level of complexity of these xerogels is very high. In all the compounds the triflate ions exist "free", weakly coordinated and forming cross-link separated ion pairs. At $20 \geq n \geq 5$, in addition to all these species contact ion pairs occur. In agreement with these conclusions, photoluminescence establishes the presence of three distinct cation local sites (Eu^{3+}/O═C(urethane cross-links), Eu^{3+}/O−C−C(polyether chains) and weakly coordinated $Eu^{3+}/CF_3SO_3^-$ ionic pairs).

Introduction

The *urethanesils* are sol−gel derived organic/inorganic materials composed of poly(oxyethylene) (POE) chains covalently bonded to a siliceous network by means of urethane (−NHC(═O)O−) moieties.[1−6] These xerogels were introduced with the primary goal of serving as model compounds of a class of advanced nanohybrids known as *di-ureasils*.[7]

In the host matrix of the di-ureasils POE segments are grafted at both ends to a siliceous backbone through urea (−NHC(═O)NH−) groups. Classical doping procedures with adequate salt species transform these POE/siloxane composites into excellent candidates for the fabrication of multipurpose, one-material-based devices. The di-ureasils incorporating lanthanide ions represent one of the best examples of the relevance of the di-ureasil strategy for the production of materials with interest for solid-state electrochemistry,[8−10] optics[8,11−18] and magnetism.[19] Their behavior is intimately associated with the combination of several factors: (1) The di-urea cross-linked host framework possesses a unique coordinating ability toward cations, since the activation of its donor centers (the ether oxygen atoms of the polymer chains and the carbonyl oxygen atoms of the cross-links (2 per organic segment)) may be tailored by varying either the guest salt content at constant chain length or the length of the organic segments at constant salt concentration.[10,11,14,15,17,20] (2) The lanthanide ions have high charge/ionic radius ratios and are characterized by high coordination numbers (typically around 12).

However, the complex structure of the di-ureasils complicates a thorough understanding of the molecular and ionic coordination in the system. To investigate in more detail the salt-doped di-ureasils we introduced two classes of structurally simpler hybrid analogues:

(1) the *di-urethanesils*,[2,5,6] in which the cross-links contain only one N−H group and are represented by the notation d-Ut-(Y) (where d denotes di, Ut indicates the urethane group and Y = 600 or 300 is the average molecular weight of the poly-(ethylene glycol) precursor, corresponding to $x \approx 13$ or 6, respectively)

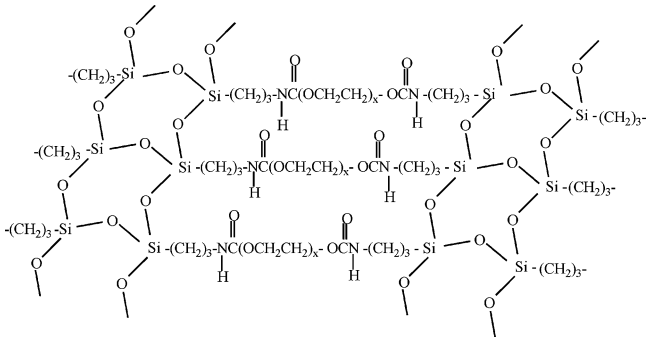

(2) the *mono-urethanesils*,[1−4] which include only one cross-link per POE segment and are represented by m-Ut(Y′) (where m denotes mono and Y′ = 750 or 350 is the average molecular weight of the poly(ethylene glycol) methyl ether precursor, corresponding to $x' \approx 17$ or 7, respectively).

* Corresponding author phone: 351-259-350253; fax: 351-259-350480; e-mail: vbermude@utad.pt.
† Universidade de Trás-os-Montes e Alto Douro.
‡ Chalmers University of Technology.
§ Universidade de Aveiro.

10.1021/jp045660v CCC: $30.25
Published on Web 03/17/2005

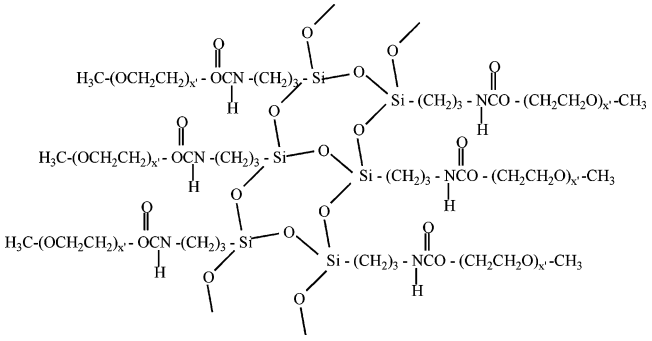

Recently we examined the optical features of d-Ut(300)-based di-urethanesils doped with $Eu(CF_3SO_3)_3$.[6] The cationic and anionic environments in these xerogels were investigated by means of FT-IR and FT-Raman spectroscopies.[6] In the present work the spectral signature of the $CF_3SO_3^-$ ion in the family of m-Ut(350)-based analogues will be analyzed using the same techniques. The interpretation of the spectra will rely on the assignment proposed for the triflate modes in the $Eu(CF_3SO_3)_3$-doped mono-urethanesil system based on the m-Ut(750) matrix.[4] We will also employ here photoluminescence spectroscopy to pursue the study of the Eu^{3+} chemical surrounding in the m-Ut-(350)-based materials already initiated.[3]

Experimental Section

Synthesis. Monourethanesil hybrids m-Ut(350)$_n$Eu$(CF_3SO_3)_3$ with $n = \infty$, 200, 100, 80, 60, 20, 10, 7 and 5 were prepared according to the procedure described elsewhere.[1−3]

FT-IR Spectroscopy. FT-IR spectra were acquired under vacuum at room temperature (RT) using a Bruker IFS-66V Fourier transform spectrometer. The spectra were collected over the range 4000−400 cm^{-1} by averaging at least 150 scans at a resolution of 2 cm^{-1}. Solid samples (2 mg) were finely ground, mixed with approximately 175 mg of dried potassium bromide (Merck, spectroscopic grade) and pressed into pellets. Viscous samples (those with $n \leq 20$) were spread on the ZnSe disks.

Prior to recording the spectra the disks were kept in an oven under vacuum at 90 °C for several days in order to reduce the levels of adsorbed water. To evaluate complex band envelopes and to identify underlying component bands of the spectra, the iterative least-squares curve-fitting procedure in the Peakfit[21] software was used extensively throughout this study. The best fit of the experimental data were obtained by varying the frequency, bandwidth and intensity of the bands. Gaussian band shapes were employed.

FT-Raman Spectroscopy. The FT-Raman spectra were recorded at RT with a Bruker IFS-66 spectrometer equipped with a FRA-106 FT-Raman module and a near-infrared YAG laser with wavelength 1064 nm. The spectra were collected over the 3200−300 cm^{-1} range at a resolution of 2 cm^{-1}. The accumulation time for each spectrum was 4 h.

2D Correlation Spectroscopic Analysis. In 2D spectroscopy, the variations in the spectra produced by an external sample perturbation are mathematically cross-correlated to construct a 2D correlation map, which allows for discrimination of those vibration modes which selectively respond to the perturbation. Two kinds of 2D spectra, defined by two independent wavenumbers (ν_1, ν_2), are generated by cross-correlation analysis of dynamic fluctuations of spectral signals induced by an external perturbation: the *synchronous* and *asynchronous* spectra.[22,23] The synchronous 2D correlation spectrum represents the simultaneous (or coincidental) changes of spectral intensities measured at ν_1 and ν_2 within the interval between T_{min} and T_{max} of the externally defined variable t, whereas the asynchronous one represents sequential (or successive) changes of spectral intensities measured at ν_1 and ν_2.

In the present work the 2D Correlation Spectroscopic Analysis was carried out using the following procedure. First, the reference spectrum was subtracted from each of the experimental spectra in order to obtain the dynamic spectra (mean-centered procedure).[22,23] For practical reasons, in our calculations the average spectrum was used as a reference. The resulting mean-centered dynamic spectra $y(\nu,t)$ represent the relative variations of spectral intensity at each wavenumber ν as a function of the lanthanide salt concentration t. We then calculated, for the set of dynamic spectra, the complex correlation function $\cdot \langle y(\nu_1,t),y(\nu_2,t')\rangle = \Phi(\nu_1,\nu_2) + i\Psi(\nu_1,\nu_2)$ using the Hilbert transform algorithm developed by Noda.[22,23] The real and imaginary parts of this function correspond to the synchronous $\Phi(\nu_1,\nu_2)$ and asynchronous $\Psi(\nu_1,\nu_2)$ 2D correlation maps of the dynamic spectra, respectively.

The synchronous 2D correlation intensities were defined by the equation

$$\Phi(\nu_1,\nu_2) = \frac{1}{n-1}\sum_{j=1}^{n} y(\nu_1,t_j)\cdot y(\nu_2,t_j) \qquad (1)$$

and the asynchronous 2D spectra were determined using the expression

$$\Psi(\nu_1,\nu_2) = \frac{1}{n-1}\sum_{j=1}^{n} y(\nu_1,t_j)\cdot \sum_{k=1}^{n} H_{jk}\cdot y(\nu_2,t_k) \qquad (2)$$

where H_{jk} is a Hilbert transformation matrix[22,23]

$$H_{jk} = \begin{cases} 0 & \text{if } j = k \\ 1/\pi(k-j) & \text{otherwise} \end{cases} \qquad (3)$$

Here ν represents the FT-IR or FT-Raman wavenumber and n is the total number of dynamic spectra. All the calculations were performed with the Matlab 6.0 software (The MathWorks Inc.).

Photoluminescence Spectroscopy. The emission (PL) and excitation (PLE) spectra were recorded between 14 K and RT on a Jobin Yvon-Spex spectrometer (HR 460) coupled to a R928 Hamamatsu photomultiplier. A Xe arc lamp (150 W) coupled to a TRIAX 180 monochromator was used as excitation source. All the spectra were corrected for the response of the detector.

Results

FT-IR and FT-Raman Spectroscopic Studies. The 18 normal modes of the "free" or nonperturbed $CF_3SO_3^-$ ion in a staggered configuration with a C_{3v} point group symmetry are sensitive to coordination effects and are thus powerful tools to probe the anionic local chemical environment. Nowadays there is a body of spectroscopic investigations devoted to the behavior of triflate anion in various POE-based polymer matrices.[24−28]

In the present work we will focus our attention on the changes undergone by the triflate bands of the m-Ut(350)-based compounds as the guest salt concentration is varied. Figures 1 and 2 show, respectively, the RT FT-IR and FT-Raman spectra of the m-Ut(350)$_n$Eu$(CF_3SO_3)_3$ mono-urethanesils in the regions that exhibit the characteristic modes of the $CF_3SO_3^-$ ion. Their frequency, intensity and attribution are given in Table 1. Because

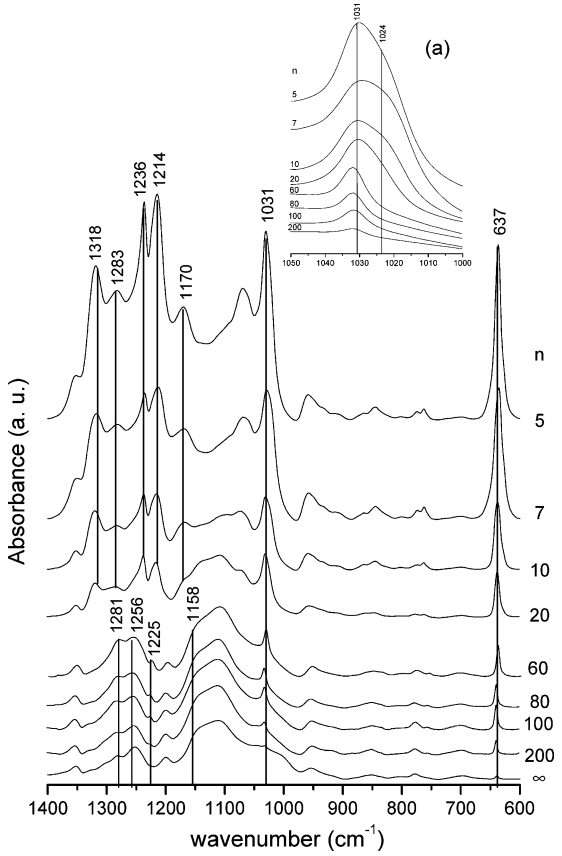

Figure 1. RT FT-IR spectra of the m-Ut(350)$_n$Eu(CF_3SO_3)$_3$ mono-urethanesils in the 1400−600 cm^{-1} region. The spectra have been scaled so that the height of the νCH_2 band is approximately the same. The inset (a) shows 1050−1000 cm^{-1} region in more detail.

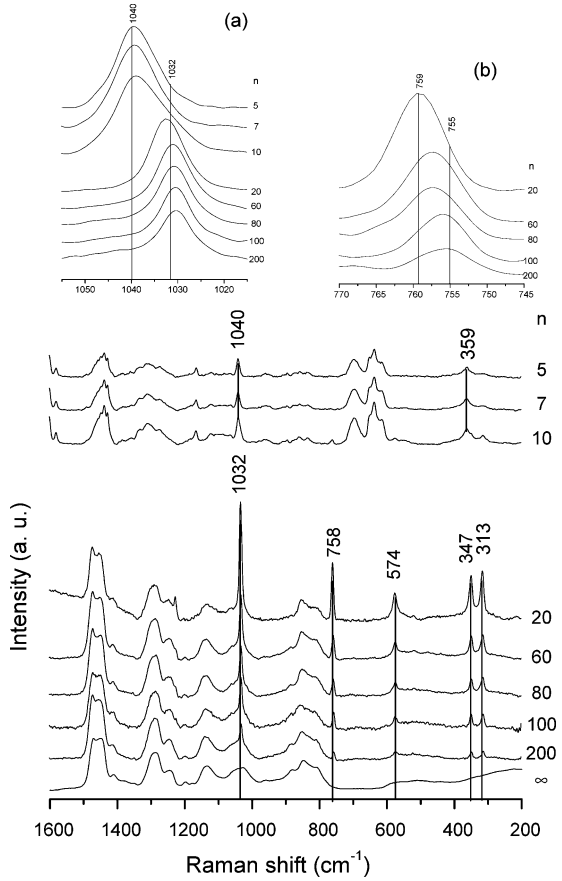

Figure 2. RT FT-Raman spectra of the m-Ut(350)$_n$Eu(CF_3SO_3)$_3$ mono-urethanesils in the 1600−200 cm^{-1} region. The spectra have been scaled so that the height of the νCH_2 band is approximately the same. The insets (a) and (b) show the 1055−1015 cm^{-1} and the 770−745 cm^{-1} regions, respectively, in more detail.

of strong overlap of different spectral bands originating from both anion and polymer, we will apply in this spectral analysis several additional procedures, such as spectra subtraction and 2D correlation spectroscopy.

$\nu_a SO_3$ Region. The asymmetric stretching vibration mode of the SO_3 group ($\nu_a SO_3$) of the "free" triflate ion occurs at 1272 cm^{-1}.[25] Cation dependent split bands appear upon coordination.[24,25,27] The width of the splitting is considered to be a good measure of the strength of the cation−anion interaction.

As the vibration modes of the POE chains of the host matrix are quite strong between 1350 and 1200 cm^{-1} (Figure 1), the identification of the triflate bands in the spectra of the doped materials is subject to much uncertainty. To unambiguously determine the spectral modifications resulting from the incorporation of Eu(CF_3SO_3)$_3$ into m-Ut(350), we subtracted the FT-IR spectrum of the nondoped hybrid from those of the materials with $200 \geq n \geq 60$. The results of this subtraction are represented in Figure 3. This procedure was not employed in the case of the samples with $20 \geq n \geq 5$, because in the latter xerogels, unlike in the more dilute ones, the POE chains bond to the Eu^{3+} ions, a process that is accompanied by marked changes in the conformations of the polymer segments.[3] It is important to note that the beginning of PEO participation in the cation coordination process is difficult to detect spectroscopically. Although FT-IR data suggest that the Eu^{3+} ions are complexed by the POE ether oxygen atoms at $n \leq 20$,[3] this threshold composition might be located at slightly lower salt content. Taking into account that there are two different types of sites in the host matrix where complexation may occur (the ether oxygen atoms of the POE chains and the carbonyl oxygen atoms of the urethane linkages), it seems plausible that at low salt contents the site with lower energy is occupied preferentially. According to the results of the analysis of the "amide I" region of the same set of mono-urethanesils studied here,[3] the Eu^{3+} ions bond to the urethane carbonyl oxygen atoms in all the samples. Thus two possible scenarios for the Eu^{3+} ion coordination in the xerogels with $n > 20$ may be envisaged: (1) the POE chains of m-Ut(350) are not involved in the complexation of the cations; (2) in this range of salt composition the number of Eu^{3+}/POE interactions is too low to influence the conformation of the polymer chains of the samples.

The data derived from the deconvolution carried out in the $\nu_a SO_3$ envelope, collected in Table 1, allow for inferring that peaks at 1308, 1289, 1272, 1259 and 1247 cm^{-1} are produced by the samples with $200 \geq n \geq 60$, whereas two new components found at approximately 1323 and 1213 cm^{-1} are discerned in the FT-IR spectra of the compounds with $20 \geq n \geq 5$.

$\nu_s SO_3$ Region. The symmetric stretching vibration mode of the SO_3 group ($\nu_s SO_3$) of a "free" triflate ion is associated with a feature situated at 1032 cm^{-1}.[29] Coordination of the $CF_3SO_3^-$ ion may shift the 1032 cm^{-1} event to higher wavenumbers,[25,28] to lower wavenumbers[24−26]and to both higher and lower wavenumbers.[24,28] In some cases, the $\nu_s SO_3$ band was found to remain unshifted.[25]

The FT-IR and FT-Raman spectra of the Eu^{3+}-doped m-Ut-(350)-based xerogels in the $\nu_s SO_3$ region are reproduced in the insets (a) of Figures 1 and 2, respectively. Close consideration of the $\nu_s SO_3$ band contour in both series of spectra shows that several components can be resolved in this region. However it

TABLE 1: Characteristic Triflate Bands of the FT-IR and FT-Raman Spectra of the m-Ut(350)$_n$Eu(CF_3SO_3)$_3$ Monourethanesils

m-Ut(350)$_n$Eu(CF_3SO_3)$_3$														POE$_n$Eu(CF_3SO_3)$_3$			
200		100		80		60		20		10		7		5			
IR	R	IR	R	IR	R	IR	R	IR	R	IR	R	IR	R	IR	R	ref 24 IR	ref 28 R	$CF_3SO_3^{-}$ [29]	attribution
								1322 S		1323 S		1324 S		1322 S		1322			anion ··· Eu^{3+} ··· polymer
1306 sh		1310 sh		1304 sh		1312 sh		1310 m		1311 m		1311 m		1308 m					NH ··· anion ··· Eu^{3+}··· O=C
1291 m		1289 m		1287 m		1288 m		1291 m		1290 m		1291 m		1289 m					anion ··· Eu^{3+} ··· urethane
1273 m		1272 m		1271 m		1271 m		1276 m		1271 m		1274 m		1276 m		1272		1273	$\nu_a SO_3$ free anion
1260 sh		1262 w		1256 w		1256 w		1257 sh		1254 sh		1259 sh		1261 sh					anion ··· Eu^{3+} ··· urethane
1248 sh		1251 sh		1244 sh		1243 sh		1245 m		1243 m		1246 m		1245 m					NH ··· anion ··· Eu^{3+} ··· O=C
								1215 S		1212 S		1212 S		1213 S		1211			anion ··· Eu^{3+} ··· polymer
1037 sh	1037 sh	1038 sh	1036sh	1037sh	1037 sh	1038 sh	1038 sh										1041		coordinated anion
1032 m	1031 m	1031 m	1031 m	1032 m	1031 S	1032 m	1031 S									1030	1032	1032	$\nu_s SO_3$ free anion
1027 sh	1024sh	1025 sh	1026 sh	1026 sh	1025 sh	1026 sh	1026 sh									1023	1021		coordinated anion
					764 sh		762 sh		763 sh								763		coordinated anion
	759 sh		759 sh		758 w		757 m		759 m										coordinated anion
	755 vw		755 w		754 sh		754 sh		755 sh								756	752	$\delta_s CF_3$ free anion

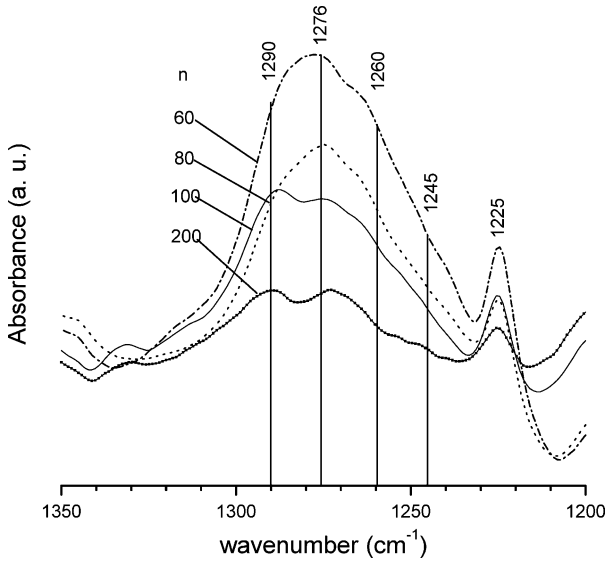

Figure 3. Subtraction RT FT-IR spectra of the m-Ut(350)$_n$Eu(CF_3SO_3)$_3$ mono-urethanesils with $200 \geq n \geq 60$ in the 1350−1200 cm^{-1} region.

is also easily recognized that the interpretation of this band envelope is not straightforward because of strong overlap between different components. This is particularly true in the case of the FT-IR spectra of the samples with $20 \geq n \geq 5$ (inset (a) of Figure 1) and in those of the FT-Raman spectra of the xerogels with $10 \geq n \geq 5$ (inset (a) of Figure 2), in which the $\nu_s SO_3$ event spans a wide range of wavenumbers. As a consequence, classical curve-fitting cannot provide alone unequivocal information about the number of components lying under the $\nu_s SO_3$ profile. This aspect induced us to carry out a deeper investigation of the $\nu_s SO_3$ feature of the FT-IR and FT-Raman spectra of the set of materials with $200 \geq n \geq 60$ by means of 2D Spectroscopic Correlation Analysis. This study will be presented below. The mono-urethanesil samples with $20 \geq n \geq 5$ were excluded from this analysis because their vibrational spectra exhibit crucial transformations originating from drastic reconfiguration of the polymer segments.[3]

$\delta_s CF_3$ Region. The symmetric deformation mode ($\delta_s CF_3$) of the CF_3 group of the "free" triflate ion was attributed to a band detected at 752 cm^{-1}.[29] When the anion is coordinated, a displacement of the $\delta_s CF_3$ modes to higher frequencies occurs.[29]

The $\delta_s CF_3$ band of the FT-Raman spectra is depicted in the inset (b) of Figure 2. The results of the curve-fitting performed in this range of wavenumbers with the latter series of spectra are summarized in Table 1. The resolved FT-Raman $\delta_s CF_3$ components derived from this procedure for representative hybrid materials are depicted in Figure 4.

Figure 4 shows that at $n = 200$ and 100 the FT-Raman spectral profile has two well-resolved peaks situated at 755 and 759 cm^{-1}. At $n = 60$ a new high-frequency component appears near 763 cm^{-1}. When composition reaches $n = 20$, the mode at 759 cm^{-1} becomes the strongest one, although "free" ions can still be detected. No studies of the FT-Raman $\delta_s CF_3$ feature of the more concentrated xerogels ($10 \geq n \geq 5$) were possible because of the low intensity and poor quality of the band contour (Figure 2).

2D Spectroscopic Correlation Analysis. To assess the changes that take place in the $\nu_s SO_3$ envelope as a function of guest salt concentration, we carried out a 2D Correlation FT-IR and FT-Raman spectroscopic study of the m-Ut(350)$_n$Eu(CF_3SO_3)$_3$ composites with $200 \geq n \geq 60$. We must draw the attention to the fact that, the samples with higher salt concentra-

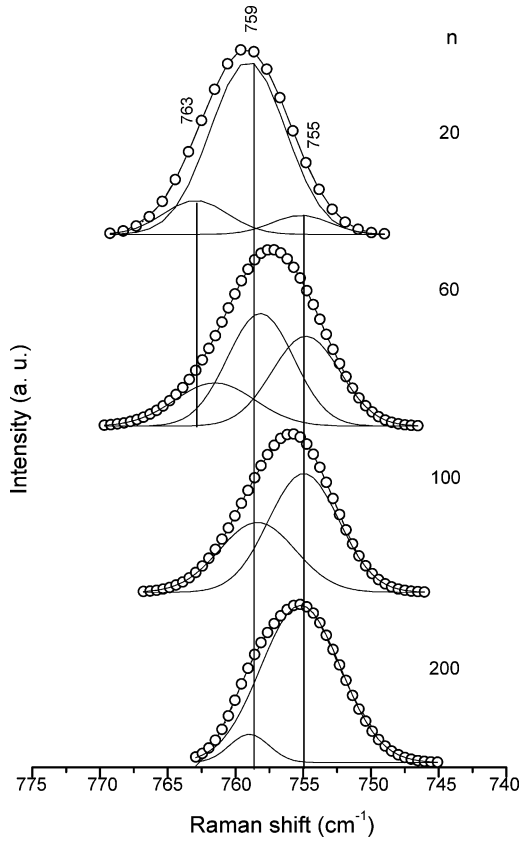

Figure 4. Curve-fitting results of the RT FT-Raman spectra of selected m-Ut(350)$_n$Eu(CF$_3$SO$_3$)$_3$ mono-urethanesils in the δ_sCF$_3$ region. For $200 \geq n \geq 60$, the subtraction spectra were used.

tion were discarded from this analysis, as the ν_sSO$_3$ profiles are significantly modifed (insets (a) of Figures 1 and 2).

The main goal of 2D Correlation Vibrational Spectroscopy is to detect dynamic variations of spectroscopic signals induced by an external perturbation, which in the present case was the addition of different amounts of Eu(CF$_3$SO$_3$)$_3$ to the m-Ut(350) framework. In dynamic vibrational spectra, typical changes in the bands are intensity variations, frequency shifts and shape modifications. The detected spectral change is then transformed in the 2D spectra by means of a specialized correlation method, such as the one described in detail in the Experimental Section. As a result of this transformation, one obtains two 2D correlation spectra usually designated as synchronous and asynchronous maps. Correlation peaks appearing in the synchronous and asynchronous maps represent in-phase and out-of-phase variation tendencies of corresponding band intensities, respectively. Finally, it should be stressed that 2D correlation analysis is particularly useful for the determination of the number of spectral components in strongly overlapped profiles.[22,23]

The asynchronous 2D correlation contour map constructed from the FT-IR spectra of the m-Ut(350)-based mono-urethanesils in the ν_sSO$_3$ region for the $200 \geq n \geq 60$ composition range is reproduced in Figure 5(a). The corresponding experimental (one-dimensional) spectra are also included at the left and top of this plot. The asynchronous map displays four cross-peaks, two of positive and two of negative intensity. By extending lines from the pair of corresponding cross-peaks to the diagonal line, it is possible to determine the spectral positions with the maximum intensity variations, i.e., the frequency positions of overlapping spectral bands.[22,23] Thus we may deduce from this plot that in the investigated ν_sSO$_3$ envelope there are three distinct components located at 1029, 1031 and 1035 cm^{-1}. The signs of the asynchronous cross-peaks at the spectral positions (1031, 1029) and (1031, 1035) are both positive. The sign peak rules[22,23] suggest that the intensity change of the 1031 cm^{-1} component occurs before that of the features at 1029 and 1035 cm^{-1}. We must mention that the peak signs of the corresponding synchronous map (not shown) at the same spectral positions are all positive.

Figure 5(b) shows the asynchronous 2D correlation map obtained from the experimental FT-Raman spectra of the m-Ut-(350)$_n$Eu(CF$_3$SO$_3$)$_3$ materials with $200 \geq n \geq 60$ in the same spectral region. This map allows for distinguishing four distinct components located at 1037, 1034, 1030 and 1026 cm^{-1}. On the basis of a previous attribution,[4] the two side peaks at 1026 and 1037 cm^{-1} may be assigned to the ν_sSO$_3$ vibration of weakly coordinated triflate ions. The appearance of two additional features at 1030 and 1034 cm^{-1} is, however, in disagreement with all known results. Usually, in this region only one peak at about 1031 cm^{-1}, associated with "free" triflate ions, should be found.[29]

We note that such an effect, i.e., the occurrence in an asynchronous 2D correlation map of two (or more) distinct components when only one band is expected, may be produced when a single peak simultaneously undergoes intensity growth and frequency shift.[30,31] It was reported in the literature that a relatively large band shift (about 7 cm^{-1}) results in a series of cross-peaks in the asynchronous 2D spectrum,[30] whereas even a very small shift of a single band (less than 2 cm^{-1}) always gives rise to two peaks regardless of the extent of the intensity changes and the selection of the reference spectrum.[31] The pattern of such features is very similar to that of two overlapped bands changing their intensity at different rates − a situation that significantly complicates the interpretation of 2D correlation map.

To clarify the origin of the alterations observed in 2D asynchronous map of the ν_sSO$_3$ region of m-Ut(350)$_n$Eu(CF$_3$-SO$_3$)$_3$ compounds with $200 \geq n \geq 60$, we constructed the asynchronous 2D correlation maps for two scenarios of peaks behavior considered to be very relevant. In the first case, illustrated in Figure 5(c), the asynchronous 2D correlation map was generated from the sequence of simulated spectra containing *four* Gaussian peaks subject to changes in their relative intensity at fixed frequency positions deduced from the experimental asynchronous 2D map (i.e., 1037, 1034, 1030 and 1026 cm^{-1}). The second map, reproduced in Figure 5(d), was obtained from the sequence of model spectra built from *three* Gaussian profiles, two of which (1037 and 1026 cm^{-1}) behave exactly like those of the previous case, whereas the strongest peak, in addition to undergo intensity growth, is slightly shifted (from 1030.5 to 1031 cm^{-1}) but displays no significant broadening (from 6.5 to 7 cm^{-1}).

We may deduce from the comparison of the experimental (Figure 5(b)) and simulated (Figures 5(c) and 5(d)) 2D spectra that the second scenario matches the experimental case better. However, in the present case a comparison based only on the asynchronous 2D maps is insufficient for a complete elucidation of the origin of the spectral changes. An additional parameter that can also be employed to clarify the nature of the peaks observed in 2D correlation spectra is the ratio of intensities of the synchronous and asynchronous peaks. It was demonstrated that this value is sensitive to the specific character of the spectral changes.[30] Thus, when 2D peaks are caused by only intensity change of the experimental band, the height of synchronous peaks is significantly larger than that of the corresponding asynchronous peak. However, when a 2D peak is due to both

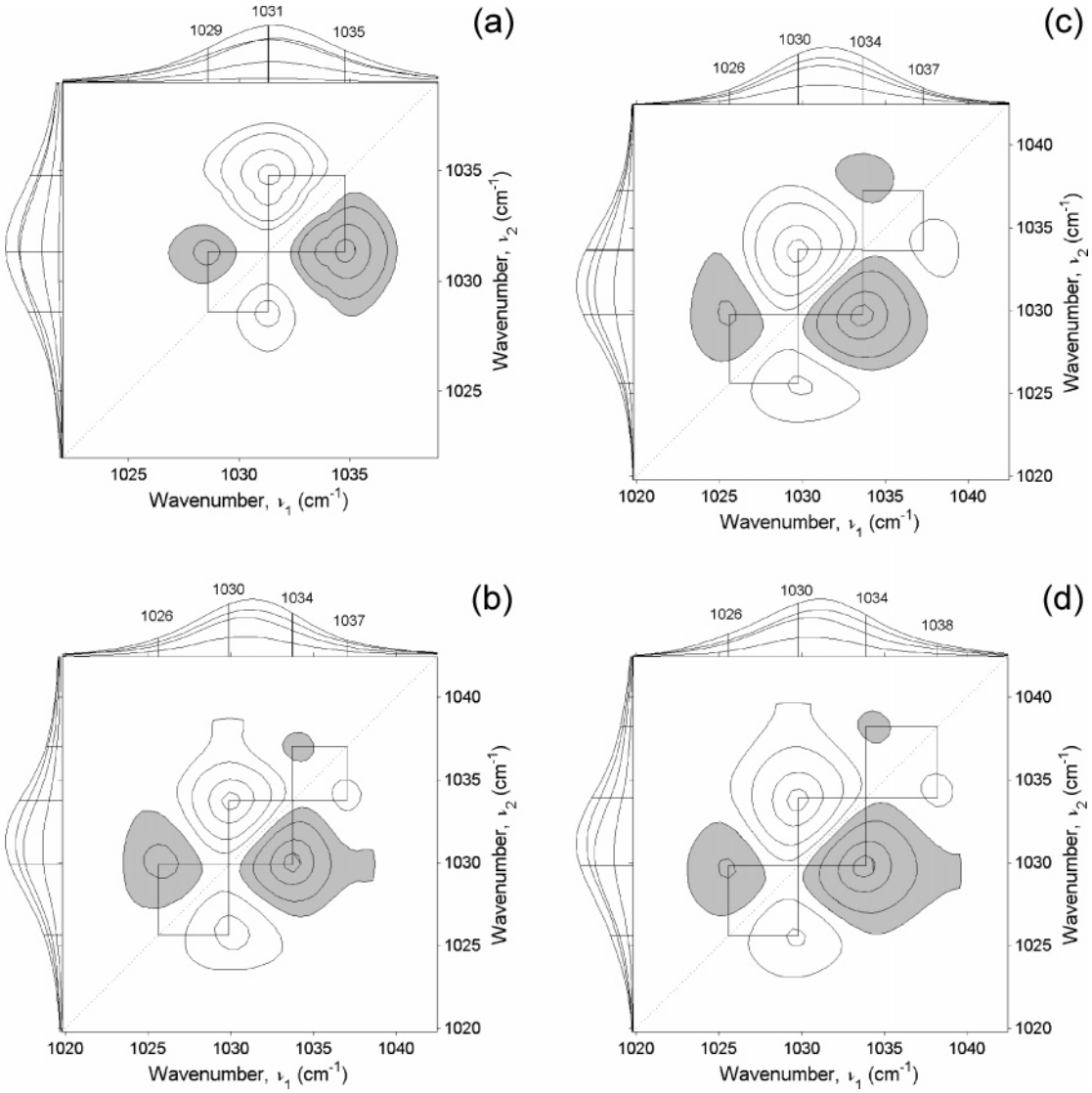

Figure 5. 2D correlation asynchronous maps constructed from (a) − experimental FT-IR spectra of the samples with $200 \geq n \geq 60$; (b) − experimental FT-Raman spectra of the samples with $200 \geq n \geq 60$; (c), (d) − simulated spectra obtained with different scenarios of peaks behavior (see text for details). Shaded areas indicate the negative correlation intensity.

intensity growth and moderate band shift, the corresponding intensity ratio is considerably lower.[30] In all the three situations examined here (the experimental and the two model ones; spectra not shown) the synchronous 2D correlation map exhibits a single auto-peak at 1030−1031 cm^{-1}. However, the ratio between its relative intensity and the intensity of the strongest asynchronous cross-peak located at (1030, 1034 cm^{-1}) was quite different. While in the experimental asynchronous 2D correlation map this ratio was found to be equal to 7, the values obtained for the simulated asynchronous 2D correlation maps were approximately 21 and 8 for the first and second models, respectively.

Hence the comparison between the experimental asynchronous 2D plot for the FT-Raman spectra of the $\nu_s SO_3$ band in the investigated mono-urethanesils with the simulated analogue plots, as well as the confrontation of the intensity ratios of the synchronous and asynchronous peaks, indicate that the spectral modifications detected are consistent with the occurrence of a shift in a single spectral component, rather than with the presence of two peaks whose relative intensities change.

On the basis of the information retrieved from 2D spectroscopic analysis, in materials with $200 \geq n \geq 60$ the FT-IR and FT-Raman $\nu_s SO_3$ band profiles were decomposed into a medium intensity feature located around 1032 cm^{-1} and two weak peaks centered near 1038 and 1026 cm^{-1} (Figure 6(a), Table 1) and a medium intensity feature located around 1032 cm^{-1} and two weak peaks centered near 1038 and 1026 cm^{-1} (Figure 6(b), Table 1), respectively.

Photoluminescence Spectroscopy. Figure 7 shows the RT PL spectra obtained for the m-Ut(350)$_n$Eu(CF_3SO_3)$_3$ mono-urethanesils with $n = 200$, 20 and 5 recorded under the excitation wavelength that maximizes the luminescence intensity (395 nm). All the spectra exhibit a large broad band between 400 and 600 nm, which is overlapped by a series of straight lines in the orange-red spectral region. These lines correspond to the Eu^{3+} intra-4f [6] transitions between the $^5D_0$ and the $^7F_{0-4}$ levels. The large broad band was also observed in the nondoped hybrid (not shown) and in other structurally similar hybrids, classed as di-ureasils and di-urethanesils.[6,13,32−35] It was demonstrated that this emission results from the convolution of two singular components attributed to radiative recombinations typical of donor−acceptor pairs, which occur in the NH groups of the cross-links (urea or urethane) and in the siliceous nanodomains, respectively.[6,13,32−35] It was recently proposed that the mechanism responsible for the NH-related component is associated with photoinduced proton-transfer between NH_2^+ and

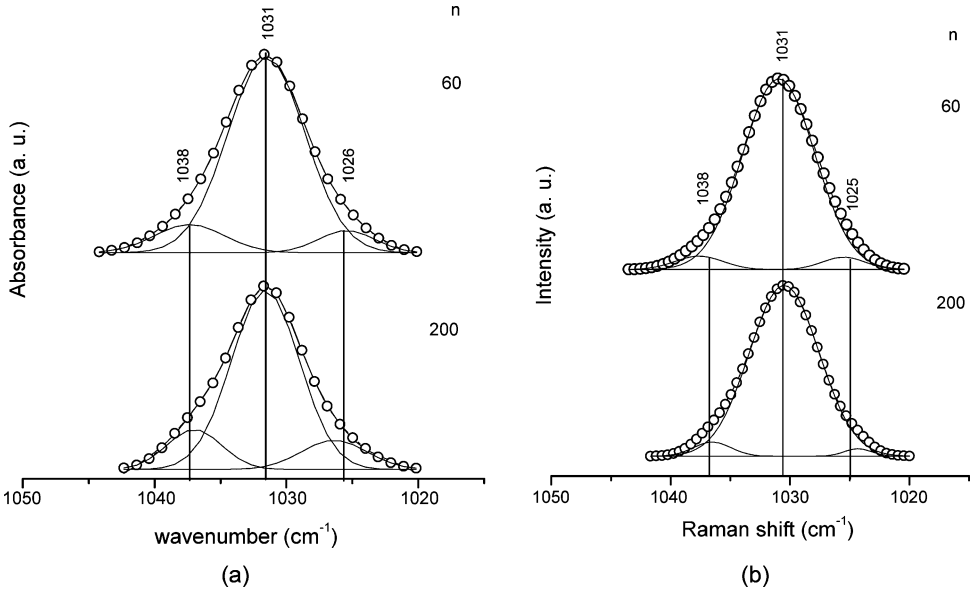

Figure 6. Curve-fitting results of the RT FT-IR (a) and FT-Raman (b) spectra of selected m-Ut(350)$_n$Eu(CF$_3$SO$_3$)$_3$ mono-urethanesils in the ν_sSO$_3$ region. To examine exclusively the contribution of the ν_sSO$_3$ mode, the FT-Raman spectrum of the pure polymer had to be first subtracted from those of the hybrids with $200 \geq n \geq 60$.

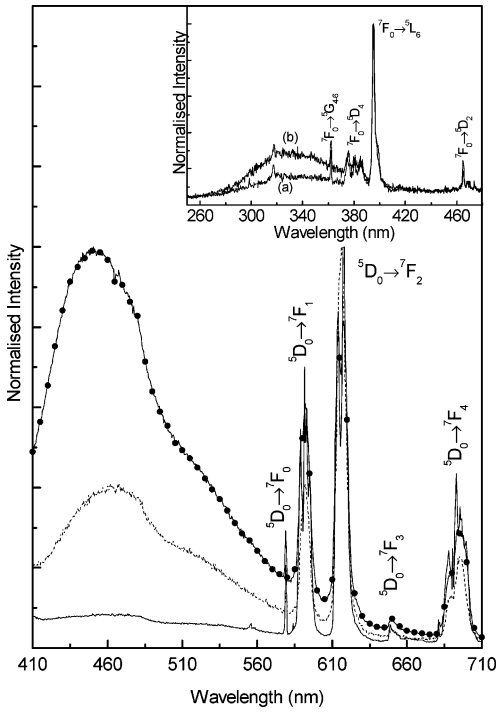

Figure 7. RT PL spectra for the m-Ut(350)$_n$Eu(CF$_3$SO$_3$)$_3$ mono-urethanesils with $n = 200$ (solid line with circles), $n = 20$ (dashed line) and $n = 5$ (solid line), excited at 395 nm. The inset shows the RT PLE spectra of the m-Ut(350)$_5$Eu(CF$_3$SO$_3$)$_3$ mono-urethanesil monitored around the $^5D_0 \rightarrow {}^7F_1$ lines, 591.5 nm (a) and around the $^5D_0 \rightarrow {}^7F_2$ transition, 613.7 nm (b).

N^- defects, whereas the PL mechanism subjacent to the component associated with the siliceous nanodomains involves oxygen-related defects, $\bullet O-O-Si\equiv(CO_2)$.[35]

The relative intensity between the hybrid host emission band and the Eu^{3+} ion lines strongly depends on the cation concentration. As Figure 7 exemplifies, while for the most concentrated sample ($n = 5$) the Eu^{3+} lines are more intense that the broad band, for the most dilute sample ($n = 200$) the opposite situation is observed. The dependence of the relative intensity between the hybrid host band and the Eu^{3+} emission is probably associated with the activation/deactivation of the energy transfer processes that take place between the mono-urethanesil emitting centers (donors) and the lanthanide ions (acceptors), similarly to what has been recently demonstrated for a series of Eu^{3+}- and Nd^{3+}-based di-ureasil and di-urethanesil hybrids.[6,16,18]

The inset of Figure 7 shows the RT PLE spectra detected around the Eu^{3+} $^5D_0 \rightarrow {}^7F_{1,2}$ lines for the m-Ut(350)$_5$Eu(CF$_3$SO$_3$)$_3$ hybrid. The spectra are composed of a large broad band between 280 and 400 nm, peaking around 341 nm, that is overlapped by a series of sharp lines assigned to intra-4f ^{6} transitions between the $^7F_0$ and the $^5G_{4-6}$, $^5L_6$, $^5D_{4,2}$ levels. For the less concentrated samples ($n \geq 20$) we observe a red-shift of the large broad band, which is now centered around 350 nm. As Figure 7 demonstrates, the relative intensity between this band and the intra-4f ^{6} lines decreases when the monitoring wavelength changes from 614 to 591 nm. The origin of this band can be ascribed to a ligand-to-metal charge transfer (LMCT) transition resulting from the interaction between the ligands and the lanthanide ions, similarly to what has been suggested for other Eu^{3+}-based organic−inorganic hybrids.[6,12,16]

Figure 8 shows in detail the low-temperature $^5D_0 \rightarrow {}^7F_{0-4}$ sharp lines typical of the Eu^{3+} energy level structure. Comparison of the PL features of the three hybrids allows for detecting changes in their energy, maximum splitting, full width at half-maximum (fwhm) and profile, in particular for the $^5D_0 \rightarrow {}^7F_{0-2,4}$ transitions. The $^5D_0 \rightarrow {}^7F_{3,4}$ transitions will be excluded from the following study due to the high number of Stark components that render difficult a detailed analysis and to the low intensity of the $^5D_0 \rightarrow {}^7F_3$ transition. The energy of the $^5D_0 \rightarrow {}^7F_0$ transition and its fwhm increases from 17253.0 to 17266.8 cm^{-1} and from 19.8 to 26.9 cm^{-1}, respectively, as the concentration varies from $n = 200$ to 5. Variations on the energy of the $^5D_0 \rightarrow {}^7F_0$ transition and the increase in its fwhm with the increase of the Eu^{3+} content readily suggest changes in the Eu^{3+} local coordination site. As Figure 8 shows there are at least 5 clearly discernible components for the $^5D_0 \rightarrow {}^7F_1$ transition, an indication of the existence of at least two Eu^{3+} local coordination sites, as the maximum splitting for the $^7F_1$ manifold (2J+1) corresponds to three Stark components. These two Eu^{3+}-local sites will afterward be identified as sites A and B. However, the spectra of the remaining transitions, in

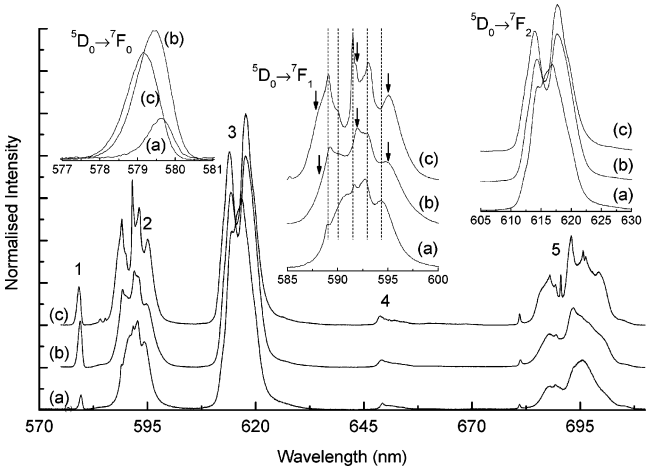

Figure 8. Low-temperature (14 K) PL spectra for the m-Ut(350)$_n$Eu(CF$_3$SO$_3$)$_3$ mono-urethanesils with $n = 200$ (a), $n = 20$ (b) and $n = 5$ (c) excited at 395 nm. (1), (2), (3), (4) and (5) represent the intra-4f ^{6} transitions: $^5D_0 \rightarrow {}^7F_{0-4}$, respectively.

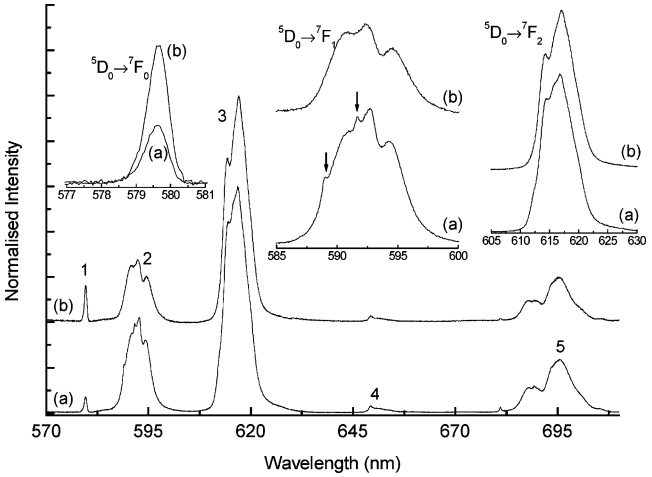

Figure 9. Low-temperature (14 K) PL spectra for the m-Ut(350)$_{200}$Eu(CF$_3$SO$_3$)$_3$ mono-urethanesil, excited around 395 nm (a) and 350 nm (b). (1), (2), (3), (4) and (5) represent the intra-4f ^{6} transitions: $^5D_0 \rightarrow {}^7F_{0-4}$, respectively.

particular that of the $^5D_0 \rightarrow {}^7F_2$ transition, do not reveal a number of Stark components compatible with two distinct Eu^{3+}-local environments, suggesting that one of the Eu^{3+}-local sites is characterized by an inversion center (site B). A similar result was reported for the d-Ut(300)$_n$Eu(CF$_3$SO$_3$)$_3$ urethanesils.[6]

Figure 9 shows the low-temperature m-Ut(350)$_{200}$Eu(CF$_3$SO$_3$)$_3$ emission spectra recorded under two different excitation wavelengths: (i) around the maximum intensity of the LMCT band (350 nm) and (ii) direct excitation of the Eu^{3+} levels, namely $^5L_6$ level (395 nm). The energy of the $^5D_0 \rightarrow {}^7F_0$ transition and its fwhm excited at 350 nm are identical to the values found for the 395 nm excitation wavelength (17252.2 and 18.2 cm^{-1}, respectively). In contrast, marked changes are detected in the $^5D_0 \rightarrow {}^7F_1$ transition as the excitation wavelength decreases from 395 to 350 nm, since only three of the five Stark components observed at 395 nm could be detected. Moreover an increase in its relative intensity regarding the remaining transitions is observed. These results indicate that the emission arising from Eu^{3+}-site B is favored for direct excitation into the intra-4f ^{6} levels, while the lanthanide ions in site A are mainly excited via the LMCT states involving the hybrid host contribution. Taking into account that there are no differences

TABLE 2: Energy Positions (E) and fwhm of the $^5D_0 \rightarrow {}^7F_0$ Transition of Sites A and C for the Monourethanesils m-Ut(350)$_n$Eu(CF$_3$SO$_3$)$_3$ with $n = 200$, 20 and 5

	m-Ut(350)$_n$Eu(CF$_3$SO$_3$)$_3$			
	Eu^{3+}-siteA		Eu^{3+}-siteC	
n	E (cm^{-1})	fwhm (cm^{-1})	E (cm^{-1})	fwhm (cm^{-1})
200	17253.9	19.8		
20	17257.6	21.6	17276.3	25.0
5	17260.1	19.4	17276.3	27.0

in the $^5D_0 \rightarrow {}^7F_{0,2}$ transitions relative to those in the spectrum excited at 350 nm, we may infer that Eu^{3+} site B involves a low symmetry local coordination with an inversion center and without the $^5D_0 \rightarrow {}^7F_0$ transition. This is similar to that already reported for the pure salt (Figure 11 of ref 6). We emphasize that we are not suggesting that pure salt exists in all the mono-urethanesils, but rather that the Eu^{3+}-site B might also involve coordination to the $CF_3SO_3^-$ anions.

Figure 8 shows that besides the two already discussed sites for the lanthanide ions (sites A and B), a third independent Eu^{3+}-local coordination place (site C) occurs around the concentration $n = 20$, being more evident in the most concentrated sample ($n = 5$). As already stated, the energy and the fwhm of the $^5D_0 \rightarrow {}^7F_0$ transition increases as the concentration varies from $n = 200$ to 5. Changes are also observed in the profile of the $^5D_0 \rightarrow {}^7F_{1,2}$ transitions, namely the $^5D_0 \rightarrow {}^7F_1$ transition reveal three Stark extra-components (marked with arrows in Figure 8) in the m-Ut(350)$_5$Eu(CF$_3$SO$_3$)$_3$ hybrid that were not detected in the most dilute sample ($n = 200$). Considering these findings, we can state that the Eu^{3+} ions in site C, similarly to what was referred for the lanthanide ions in site A, do not occupy a place with inversion center.

The energy and the fwhm of the two $^5D_0 \rightarrow {}^7F_0$ transitions corresponding to sites A and C were estimated by deconvolution of the overall spectra, considering a sum of two Gaussian functions. The energy and fwhm of the Gaussian function that models the $^5D_0 \rightarrow {}^7F_0$ line associated with site A were independently estimated for the m-Ut(350)$_{200}$Eu(CF$_3$SO$_3$)$_3$ hybrid. These values were considered independent of the Eu^{3+} content and only its integrated intensity and the parameters (energy, fwhm and integrated intensity) of $^5D_0 \rightarrow {}^7F_0$ transition of the Eu^{3+}-site C were free to vary. The fit results are gathered in Table 2 for the salt-rich xerogels with $n = 20$ and 5. Apart from minor shifts (<7 cm^{-1}) the energy and the fwhm of the $^5D_0 \rightarrow {}^7F_0$ transition of sites A and C are similar for all the selected samples. The $^5D_0 \rightarrow {}^7F_0$ line associated with the latter Eu^{3+} coordination presents energy blue-shift and fwhm values higher than that associated with Eu^{3+}-site A. The Eu^{3+} PL features within the concentration range $200 \geq n \geq 5$ are very similar to those already reported for the d-Ut(300)$_n$Eu(CF$_3$SO$_3$)$_3$ analogues.[6]

Discussion

In the $\nu_a SO_3$ region of the m-Ut(350)-based mono-urethanesils the band observed at about 1273 cm^{-1} is ascribed to the occurrence of "free" $CF_3SO_3^-$ ions.[25] The 1323 cm^{-1}/1213 cm^{-1} pair observed in the FT-IR spectra of the m-Ut(350)$_n$Eu(CF$_3$SO$_3$)$_3$ materials with $20 \geq n \geq 5$ is attributed to the formation of contact ion pairs.[4,24] The 1308 cm^{-1}/1247 cm^{-1} pair, detected in the whole range of salt content analyzed, is assigned to cross-link separated ion pairs.[4]

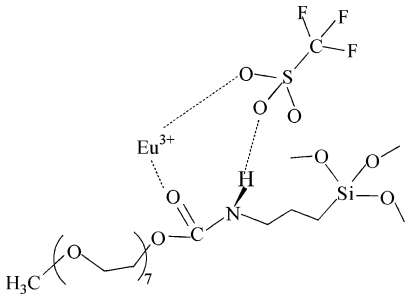

At last, the 1289 cm^{-1}/1259 cm^{-1} pair, produced by all the xerogels, corresponds to two different anionic configurations where the anions are weakly bonded:[4]

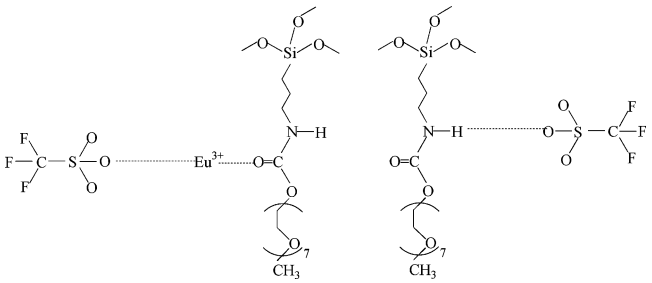

The magnitude of the splittings (ca. 110, 61 and 30 cm^{-1} (Table 1)), slightly greater than those reported for the m-Ut(750)-containing hybrids,[4] leads us to suppose that the interactions involved in the establishment of these three ionic species are stronger in the m-Ut(350)-based hybrids than in the higher molecular weight analogues.

The 755 and 759 cm^{-1} peaks detected in the FT-Raman spectra of the materials with $200 \geq n \geq 20$ are associated with noncoordinated and coordinated triflate ions, respectively.[29] The new FT-Raman feature at 763 cm^{-1} for $80 \geq n \geq 20$ suggests that a second coordinating site exists for the triflate ions in this range of salt composition.

The conclusion retrieved from the examination of the $\nu_a SO_3$ and $\delta_s CF_3$ regions that "free" triflate ions are present in the mono-urethanesils is corroborated in the $\nu_s SO_3$ region by the appearance of the band characteristic of the nonperturbed mode at approximately 1032 cm^{-1} in the FT-IR and FT-Raman spectra of all the samples synthesized (Figures 1 and 2, respectively, Table 1). The two shoulders visible on both sides of the 1032 cm^{-1} feature in the FT-IR (Figure 6(a), Table 1) and FT-Raman (Figure 6(b), Table 1) spectra of the hybrids with $200 \geq n \geq 60$ are associated with the existence of the weakly coordinated anions located in two distinct sites. The intensity ratio between the 1032 cm^{-1} component and the two shoulders informs that the concentration of "free" anions in these mono-urethanesils is much higher than that of the coordinated species. This result is consistent with the peak sign analysis of the 2D correlation maps built with the FT-IR spectra of the mono-urethanesils in the $\nu_s SO_3$ region.

The investigation of the $\nu_a SO_3$ band of the m-Ut(350)$_n$Eu-$(CF_3SO_3)_3$ hybrids with $n > 20$ indicates the presence of three different anionic environments, instead of the two deduced from the study of the $\nu_s SO_3$ envelope (Table 1). On the basis of the studies of Petersen et al.,[28] we propose that the 1032 cm^{-1} $\nu_s SO_3$ component of the m-Ut(350)-based xerogels receives contributions from not only the "free" $CF_3SO_3^-$ ions but also from the cross-link separated ion pairs.

The fact that the CF_3 end of the triflate ion in the m-Ut-(350)-based hybrids must be considerably less perturbed by the establishment of cation−anion interactions than the SO_3 end may explain why in compounds with $200 \geq n \geq 60$ composition the anionic configurations deduced from the study of the $\nu_a SO_3$ and $\nu_s SO_3$ envelopes (three, i.e., cross-linked separated ion pairs and two weakly coordinating configurations) outnumber those deduced from the analysis of the $\delta_s CF_3$ mode (one for m-Ut-$(350)_{200}Eu(CF_3SO_3)_3$ and m-Ut$(350)_{100}Eu(CF_3SO_3)_3$ and two for samples with $n = 80$ and 60).

The present analysis proves that the degree of complexity of the m-Ut$(350)_nEu(CF_3SO_3)_3$ composites is much higher than that of the m-Ut(750)-based parent analogues from the standpoint of ionic association. Although in both types of systems weakly coordinated anions are immediately formed at the lowest salt concentrations considered ($n = 200$ and 400,[4] respectively), in the low molecular weight mono-urethanesils the occurrence of the cross-linked separated ion pairs is detected already at $n = 200$, whereas in the m-Ut$(750)_nEu(CF_3SO_3)_3$ family these ionic aggregates are only formed at $n \leq 30$.[4] In both categories of hybrids, independently of the $Eu(CF_3SO_3)_3$ content, noncoordinated anions are always present. The formation of ion contact pairs is concomitant with the coordination of the lanthanide ions to the ether oxygen atoms of the POE segments.

The most important conclusions derived from the photoluminescence measurements regard the Eu^{3+} chemical surrounding. It was demonstrated that for the more diluted samples ($n > 20$), two independent Eu^{3+} coordination places exist (sites A and B).

The point symmetry group of Eu^{3+} in site B has an inversion center, and the chemical nature of its first coordination sphere involves weakly coordinated $Eu^{3+}/CF_3SO_3^-$ ionic species. This claim is in agreement with the conclusions drawn from the FT-IR and FT-Raman spectroscopic data discussed above.

The local environment of the cations in sites A ($200 \geq n \geq 5$) and C ($20 \geq n \geq 5$) is distinct from that of site B. These two local environments do not involve a point symmetry group with an inversion center and might encompass hybrid host groups. The PLE spectra of all the samples analyzed (inset of Figure 7) show the presence of a LMCT band that is related with the Eu^{3+}-ligands interaction, whose intensity is favored with respect to the cation lines for monitoring wavelengths around the $^5D_0 \rightarrow {}^7F_2$ transition than for detection wavelengths in the $^5D_0 \rightarrow {}^7F_1$ emitting region. We may thus conclude that the Eu^{3+} ions in sites A and C must directly interact with the hybrid host. The possible mono-urethanesil coordinating groups involve the oxygen atoms of the urethane carbonyl moieties and the oxygen atoms of the POE chains. Further information regarding the nature of the Eu^{3+}-site A and -site C can be extracted from the analysis of the PLE spectra as the concentration increases from $n = 200$ to 20 and 5. The m-Ut$(350)_{200}Eu(CF_3SO_3)_3$ nanohybrid presents a LMCT band at lower energy (350 nm, 28570 cm^{-1}) than those displayed by the m-Ut$(350)_nEu(CF_3SO_3)_3$ samples with $n = 20$ and 5 (341 nm, 29325 cm^{-1}). It is known that a shift of the LMCT transition frequencies toward the high-energy region of the spectrum is related with an increase of the effective charge of the lanthanide ion, and, thus, to a decrease of the tendency of the first shell ligands to bond covalently to the metal ion.[12,16] Therefore, this suggests that the Eu^{3+} ions experience a more covalent environment in site A than that in site C.

The energy of the $^5D_0 \rightarrow {}^7F_0$ transition is usually correlated with the so-called *nephelauxetic* effect induced by the ion first neighbors,[36,37] in such a way that a red-shift of the $^5D_0 \rightarrow {}^7F_0$ transition is correlated with the Eu^{3+} local sites whose first coordination sphere has a greater covalency degree.[12,14,15−17,36,37] Taking into account that the oxygen atoms from carbonyl groups

have a higher tendency to bond covalently to the metal ion than those of the POE chains,[12,14,15−17,36] we may suggest that the Eu^{3+} ions in sites A and C interact mainly with the carbonyl-type oxygen atoms and with the ether-type oxygen atoms, respectively:

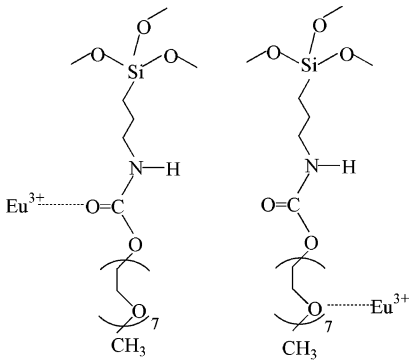

This conclusion derived from the PL and PLE data is in agreement with previous conclusions that indicated that, while the Eu^{3+} ions are coordinated to the urethane carbonyl moieties in the whole range of salt composition, only at $n < 60$ the coordination to the oxygen atoms of the POE chains occurs.[3] The three Eu^{3+} local coordination sites discussed here were also proposed for the d-Ut(300)$_n$Eu$(CF_3SO_3)_3$ di-urethanesil hybrids.[6]

Conclusions

The present FT-IR and FT-Raman spectroscopic study of ion association in *mono-urethanesil*s doped with $Eu(CF_3SO_3)_3$ pointed out the presence of "free" $CF_3SO_3^-$ ions, weakly coordinated anions located in two different sites and cross-link separated ion pairs over the whole range of salt composition examined ($\infty > n \geq 5$). At $20 \geq n \geq 5$, "free" ions, the ionic configurations detected at lower salt concentration and contact ion pairs coexist.

The high number of anionic sites found in the m-Ut(350)$_n$Eu-$(CF_3SO_3)_3$ family originate very likely, not only from the rich coordinating possibilites offered by trivalent triflate salts but also from the low molecular weight of the POE chains of the m-Ut(350) host material.

In agreement with these conclusions and those retrieved from a previous study,[3] the PL and PLE data establish the presence of three distinct cation local sites in the m-Ut(350)$_n$Eu$(CF_3$-$SO_3)_3$ compounds. Such hybrids exhibit Eu^{3+} local configurations similar to those present in structurally more complex systems as the di-urethanesils, thus suggesting that they can be used as cation local coordination models in this type of organic/inorganic hybrids.

Acknowledgment. This work has been supported by Fundação para a Ciência e Tecnologia (POCTI/P/CTM/46780/03). D. Ostrovskii and S. Lavoryk acknowledge financial support from MISTRA program and Svenska Institute, respectively.

References and Notes

(1) De Zea Bermudez, V.; Gonçalves, M. C.; Carlos, L. D. *Ionics* **1999**, *5* (3&4), 251.
(2) Gonçalves, M. C.; De Zea Bermudez, V.; Ostrovskii, D.; Carlos, L. D. *Ionics* **2002**, *8* (1&2), 62.
(3) Gonçalves, M. C.; De Zea Bermudez, V.; Ostrovskii, D.; Carlos, L. D. *J. Mol. Struct*. **2002**, *611* (2−3), 83.
(4) De Zea Bermudez, V.; Ostrovskii, D.; Lavoryk, S.; Gonçalves, M. C.; Carlos, L. D. *Phys. Chem. Chem. Phys*. **2004**, *6*, 649.
(5) Carlos, L. D.; Sá Ferreira, R. A.; Gonçalves, M. C.; De Zea Bermudez, V. *J. Alloys Compds* **2004**, *374*, 50.
(6) Gonçalves, M. C.; De Zea Bermudez, V.; Sá Ferreira, R. A.; Carlos, L. D.; Ostrovskii, D.; Rocha, J. *Chem. Mater*. **2004**, *16* (13), 2530.
(7) Armand, M.; Poinsignon, C.; Sanchez, J.-Y.; De Zea Bermudez, V. U.S. Patent, 5,283,310, 1994.
(8) De Zea Bermudez, V.; Carlos, L. D.; Duarte, M. C.; Silva, M. M.; Silva, C. J.; Assunção, M.; Alcácer, L. *J. Alloys Compds* **1998**, *275−277*, 21.
(9) Silva, M. M.; De Zea Bermudez, V.; Carlos, L. D.; Passos de Almeida, A. P.; Smith, M. J. *J. Mater. Chem*. **1999**, *9*, 1735.
(10) Silva, M. M.; De Zea Bermudez, V.; Carlos, L. D.; Smith, M. J. *Electrochim. Acta* **2000**, *45*, 1467.
(11) Carlos, L. D.; De Zea Bermudez, V.; Sá Ferreira, R. A. *J. Non-Cryst. Solids* **1999**, *247*, 203.
(12) Carlos, L. D.; Sá Ferreira, R. A.; De Zea Bermudez, V.; Molina, C.; Bueno, L. A.; Ribeiro, S. J. L. *Phys. Rev. B* **1999**, *60* (14), 10042.
(13) Carlos, L. D.; Sá Ferreira, R. A.; Orion, I.; De Zea Bermudez, V.; Rocha, J. *J. Luminescence* **2000**, *87−89*, 702.
(14) Carlos, L. D.; Messaddeq, Y.; Brito, H. F.; Sá Ferreira, R. A.; De Zea Bermudez, V.; Ribeiro, S. J. L. *Adv. Mater*. **2000**, *12* (8), 594.
(15) De Zea Bermudez, V.; Sá Ferreira, R. A.; Carlos, L. D.; Molina, C.; Dahmouche, K.; Ribeiro, S. J. L. *J. Phys. Chem. B* **2001**, *105*, 3378.
(16) Sá Ferreira, R. A.; Carlos, L. D.; Gonçalves, R. R.; Ribeiro, S. J. L.; De Zea Bermudez, V. *Chem. Mater*. **2001**, *13*, 2991.
(17) Dahmouche, K.; Carlos, L. D.; De Zea Bermudez, V.; Sá Ferreira, R. A.; Santilli, C. V.; Craievich, A. F. *J. Mater. Chem.* **2001**, *11*, 3249.
(18) Sá Ferreira, R. A.; Carlos, L. D.; Molina, C.; De Zea Bermudez, V.; Dahmouche, K.; Messaddeq, Y.; Ribeiro, S. J. L. *J. Sol-Gel Sci. Technol.* **2003**, *26*, 315.
(19) Amaral, V.; Carlos, L. D.; De Zea Bermudez, V. *IEEE Trans. Magn.* **2001**, *37*, 2935.
(20) Dahmouche, K.; Carlos, L. D.; Santilli, C. V.; De Zea Bermudez, V.; Craievich, A. F.; *J. Phys. Chem. B* **2002**, *106*, 4377.
(21) Peakfit is a product of Jandel Corporation, 2591 Rerner Boulevard, San Rafael, CA 94901, U.S.A.
(22) Noda, I. *Bull. Am. Phys. Soc*. **1986**, *31*, 520.
(23) Noda, I.; Dowrey, A. E.; Marcott, C.; Story, G. M.; Ozaki, Y. *Appl. Spectrosc*. **2000**, *54* (7), 236A.
(24) Bernson, A.; Lindgren, J. *Solid State Ionics* **1993**, *60*, 31.
(25) Wendsjö, Å; Lindgren, J.; Thomas, J. O.; Farrington, G. C. *Solid State Ionics* **1992**, *53−56*, 1077.
(26) Bergström, P.- Å.; Frech, R. *J. Phys. Chem*. **1995**, *99*, 12603.
(27) Ferry, A.; Jacobsson, P.; Stevens, J. R. *J. Phys. Chem*. **1996**, *100*, 12574.
(28) Petersen, G.; Brodin, A.; Torell, L. M.; Smith, M. J. *Solid State Ionics* **1994**, *72*, 165.
(29) Johnston, D. H.; Shriver, D. F. *Inorg. Chem*. **1993**, *32*, 1045.
(30) Czarnecki, M. A. *Appl. Spectrosc*. **2000**, *54* (7), 986.
(31) Gericke, A.; Gadaleta, S. J.; Brauner, J. W.; Mendelsohn, R. *Biospectrosc*. **1996**, *2* (6), 341.
(32) Carlos, L. D.; Sá Ferreira, R. A.; De Zea Bermudez, V.; Ribeiro, S. J. L. *Adv. Funct. Mater*. **2001**, *11* (2), 111.
(33) Carlos, L. D.; De Zea Bermudez, V.; Sá Ferreira, R. A.; Marques, L.; Assunção, M. *Chem. Mater*. **1999**, *11*, 581.
(34) Carlos, L. D.; Sá Ferreira, R. A.; De Zea Bermudez, V. In *Handbook of Organic−Inorganic Hybrid Materials and Nanocomposites*; Nalwa, H. S., Ed.; American Scientific Publishers: Morth Lewis Way, California, 2003; Vol. 1, p 353.
(35) Carlos, L. D.; Sá Ferreira, R. A.; Pereira, R. N.; Assunção, M.; De Zea Bermudez, V. *J. Phys. Chem B* **2004**, *108*, 14924.
(36) Frey, S. T.; De Horrocks, W., Jr. *Inorg. Chim. Acta* **1995**, *229*, 383.
(37) Malta, O. L.; Batista, H. J.; Carlos, L. D. *Chem. Phys.* **2002**, *282*, 21.